Eur. Phys. J. B **29**, 561–566 (2002)
DOI: 10.1140/epjb/e2002-00340-5

THE EUROPEAN PHYSICAL JOURNAL B

$SrRuO_3$ based heterostructures grown by pulsed laser deposition

M. Angeloni, C. Aruta, G. Balestrino, P. Orgiani, A. Tebano[a], and P.G. Medaglia

INFM Coherentia - Dipartimento di Ingegneria Meccanica, Università di Roma "Tor Vergata", Via del Politecnico 1, 00133 Roma, Italy

Received 3 July 2002 / Received in final form 12 September 2002
Published online 31 October 2002

Abstract. In this report we demonstrate that high quality epitaxial heterostructures, based on metallic $SrRuO_3$ and insulating $SrTiO_3$ individual blocks a few unit cells thick, can be grown in a purely 2D, layer-by-layer mode, using pulsed laser deposition with *in situ* reflection high energy electron diffraction (RHEED) diagnostics. The thickness of each constituent block can be controlled at the level of a single unit cell. A detailed investigation carried out at the synchrotron facility, ESRF, by various X-ray techniques has demonstrated that each intensity oscillation of the RHEED specular spot corresponds strictly to the growth of a single perovskite unit cell, either $SrRuO_3$ or $SrTiO_3$. Furthermore, we show that, in these structures, the interfaces between the different constituent blocks are very sharp with a roughness of only one unit cell.

PACS. 81.15.Fg Laser deposition – 61.10.Kw X-ray reflectometry (surfaces, interfaces, films) – 68.55.Ac Nucleation and growth: microscopic aspects

1 Introduction

Heterostructures based on perovskite oxides can be relevant for future electronic and spintronic device applications. Among them, spin polarized tunnel junctions have attracted strong interest. Such devices consist of two magnetic layers separated by a thin dielectric layer grown on a suitable substrate (for example $SrTiO_3$). The dielectric barrier between the magnetic oxide layers is made of an insulating oxide with matched in-plane lattice parameters (in most cases $SrTiO_3$, $LaAlO_3$ or $NdGaO_3$). Because of the very high degree of spin polarization, typical of metallic oxides, tunnel junctions based on these materials are expected to show colossal tunnel magnetoresistance effects (see, for instance, Ref. [1]). To have a reasonable tunnel resistance, in practical devices, the barrier must be very thin, typically a few nanometers [2,3]. In real tunnel junctions, based on half metallic oxides, it has been found that tunnel magnetoresistance drops to zero well below the Curie temperature. Such an effect restricts the application of these devices to low temperatures even when the Curie point of the metallic oxide is above room temperature.

The key issue in this field is to understand whether the effect is intrinsic to the interfaces, because of the rapid decrease of surface spin polarization at the Fermi level, as indicated by photoemission work [4], or is rather the result of a non ideal deposition process which results in an inhomogeneous barrier with rough and defective interfaces [5]. In this framework, control of the deposition process at the level of a single unit cell is mandatory in order to understand the physical mechanisms of the tunnelling process in perovskite based tunnel junctions.

Recently, significant progress has been made in the layer-by-layer growth of complex oxide films and heterostructures by molecular beam epitaxy (MBE) and pulsed laser deposition (PLD) with *in situ* reflection high-energy electron diffraction (RHEED) [6–8]. It has been shown that 2D layer-by-layer growth can be achieved even for quite complex systems such as perovskite oxides. However, for this class of materials, the individual layer of the 2D deposition process does not consist of a single atomic plane but rather of a more complex structural unit, which satisfies the requirement of charge neutrality. In most cases this deposition unit coincides with the crystallographic unit cell of the compound [9–11]. The layer by layer epitaxial growth of perovskite oxides can be understood in terms of a simple model: random deposition of atoms and/or complexes, surface migration of species for reaction and, for a longer time scale, diffusion of growth units to higher coordination sites [12]. Usually, such a growth process leads to a variation of the step density on the film surface. Under suitable conditions of growth temperature, oxygen pressure and miscut angle of the substrate, this variation can be periodic in time, with the period coinciding with the time necessary for the deposition of a single layer (unit cell) of the compound. In turn this can result in a periodic oscillation of the RHEED intensity. Therefore RHEED oscillations can be used to control *in situ* the deposition with the precision of a single unit.

Here we will focus on the investigation of heteroepitaxial structures based on the $SrRuO_3$ (SRO) itinerant metallic ferromagnetic oxide. Because of its electrical and

[a] e-mail: tebano@uniroma2.it

magnetic properties [13,14] and its structural compatibility with high temperature superconductors such as $YBa_2Cu_3O_{7-\delta}$ [15], the conductive magnetic oxide SRO represents a very interesting material system not only for its fundamental physical properties but also for its potential applications [16]. In this study we show that complex heteroepitaxial structures, consisting of $SrRuO_3$ and of $SrTiO_3$ (STO) thin layers, can be engineered by PLD with *in situ* RHEED (hereafter laser MBE). RHEED allows control, through the intensity oscillations, of the exact number of unit cells deposited in each layer. This process leads to an error in the thickness of each individual layer smaller than a single unit cell. Furthermore the amplitude of RHEED oscillations during the deposition of the electrode layers has been shown to be related to the quality of the barrier in oxide tunnel junctions [5]. Furthermore we will show, by synchrotron X-ray diffraction characterization, that the roughness of each individual interface is of the order of a single unit cell (namely about 4 Å).

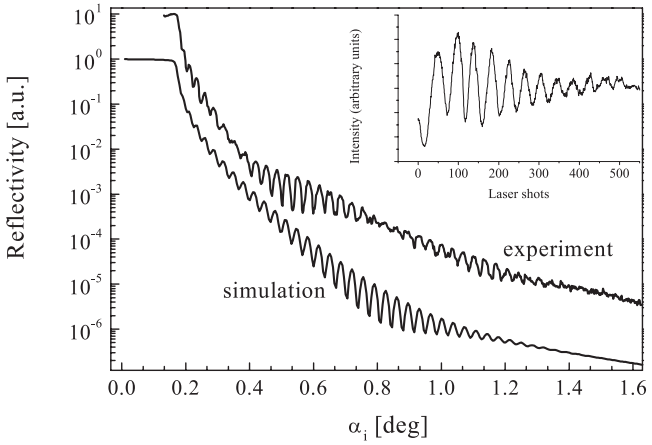

Fig. 1. X-ray reflectivity of a "thick" SRO film. In the inset the oscillations of the RHEED specular spot at the beginning of the deposition process are shown.

2 Experimental

A KrF excimer laser (λ = 248 nm) with a pulse length of 25 ns was used for the PLD growth. The laser fluence was maintained at a value of 30 mJ to obtain a growth rate of about 10^{-1} Å per laser shot. The laser repetition frequency was 1 Hz. In our experimental set-up the laser beam forms an angle of 45° relative to the target surface and the beam spot is focused to about 3 mm^2 at the target surface. Targets (one inch polycrystalline SRO and single crystal STO disks) were mounted on a computer-controlled carousel. The number of laser shots on each target was adjusted in order to grow different artificial structures. During deposition each target rotated around the perpendicular to the surface. The SRO target was prepared according to the following procedure: stoichiometric mixtures of high purity RuO_2 and $SrCO_3$ powders were calcinated at 860 °C in air for at least 24 hours. The weight loss was checked. Powders were pressed into a disk shape and then sintered for 48 hours at 1200 °C. The STO target was a commercial sample from Crystal Gmbh. STO substrates ((001) oriented with zero nominal miscut) were placed on a heated holder at a distance of about 10 cm from the target. Substrates were treated according to the recipe given in reference [17] in order to have a TiO_2 terminated surface. The growth atmosphere was a mixture of molecular oxygen and 10% of the ozone. In order to utilize the *in situ* RHEED technique, the growth pressure was maintained in 10^{-4} Pa range. The growth temperature T_g was about 600 °C. Transport properties were measured by the standard four contacts technique. The X-ray measurements were performed at the ID32 insertion device beamline at the European Synchrotron Radiation Facility (ESRF) in Grenoble, using an X-ray energy of 16 KeV selected by a silicon (111) double crystal monochromator. Vertical focusing of the beam and harmonic rejection were obtained with a Pt coated stripe of a biomorph mirror. Reflectivity and diffraction measurements were carried out with a four circle (2+2) diffractometer. Specular reflectivity measurements were carried out to determine the thickness of the constituent layers and the roughness of the surface and the interfaces. The simulation of the reflectivity curves was performed with the IMD code [18] available in the XOP package [19]. Furthermore, diffraction measurements in specular configuration, allowed us to obtain information about both the interplanar distances along the *c*-axis direction and the thickness of the constituent layers. For heterostructures such information can be obtained by simulation of the experimental profiles by theoretical curves. Simulations were performed with a computer program developed to calculate the diffraction from heterostructures with abrupt interfaces employing the dynamical X-ray diffraction formalism by Takagi and Taupin [20,21]. Finally, in-plane lattice parameters were measured in grazing incidence configuration to reduce the penetration depth of the probing X-ray beam and enhance the sensitivity to thin layers.

3 Results and discussion

As a preliminary step a SRO film, about 600 Å thick was deposited by laser MBE. During the initial stage of the growth, several clear oscillations of the specular spot of the RHEED pattern were detected. In the inset of Figure 1 the oscillations of the RHEED specular spot at the beginning of the deposition process are shown. RHEED oscillations are slightly damped and become very faint after approximately 12 cycles. However, the RHEED pattern remains 2D until the end of the deposition. This finding indicates that the growth proceeds layer-by-layer and that after the first 12 RHEED oscillations, the step density on the film surface remains roughly constant. This result is different from that obtained by Choi *et al.* [22], who observed a growth mode transition from layer-by-layer to step flow during the earliest stage of heteroepitaxial SRO films on STO substrate. The different growth mode could be ascribed to the different deposition parameters and/or the different preparation process of the

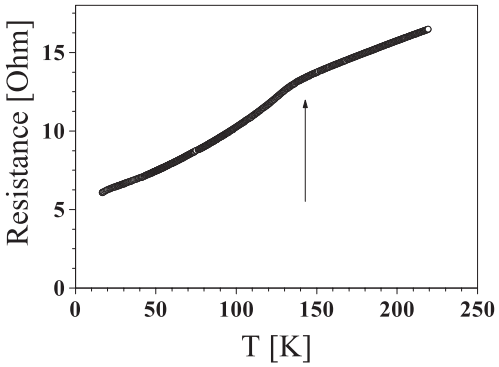

Fig. 2. Behaviour of resistance *versus* temperature for the same film of Figure 1. The arrow indicates the Curie temperature.

substrate. The oscillation period is not constant. Namely, 54 laser shots are needed to complete the first oscillation, while the period of all remaining oscillations is equal to 42 laser shots. Such an effect, already observed by different authors during the heteroepitaxial growth of complex oxides [9,22], is related to the lower surface mobility during the heteroepitaxial growth of the first layer of SRO on the STO surface relative to the homoepitaxial growth of SRO on SRO. Therefore we have calibrated the growth rate of the film, considering the value of 42 laser shots per unit cell, as 9.5×10^{-2} Å per shot. Consequently, taking into account the overall number of laser shots, the thickness of the whole film was estimated to be 616 Å. The same film was investigated by specular X-ray reflectivity. Results are shown in Figure 1. Interference fringes are clearly visible up to an angle of 1.4 degrees. The experimental data were simulated using the IMD extension of the XOP package [18,19]. The theoretical behaviour is shown in the same figure. From this simulation a film thickness of 618 ± 2 Å can be estimated, in excellent agreement with the value obtained by the RHEED oscillations. This result confirms that each RHEED oscillation corresponds strictly to the growth of a 2D layer consisting of a single unit cell of SRO. Moreover, simulation of Figure 1 allows the estimation of both the substrate and the surface roughness. The interface (substrate/film) roughness results to be negligible, while a value of 8 Å (about 2 unit cells) was found for the surface roughness. Two different oscillation frequencies can be observed in the reflected intensity. While the higher frequency oscillations depends on the thickness of the whole SRO film, the lower frequency modulation can be tentatively associated with an interface (or surface) layer about 30 Å thick. The c lattice parameter of this film, measured using the (002) diffraction peak, resulted to be 3.96 Å. Such a value is slightly larger relative to the pseudocubic bulk value of 3.93 Å commonly quoted for polycrystalline and single crystal samples. This effect, already noticed in "thick" SRO films, can be ascribed either to ion bombardment during the growth process [23], or to oxygen deficiency caused by the low oxygen growth pressure in laser MBE [24]. In Figure 2 we show the behaviour of resistance *versus* temperature for the same film

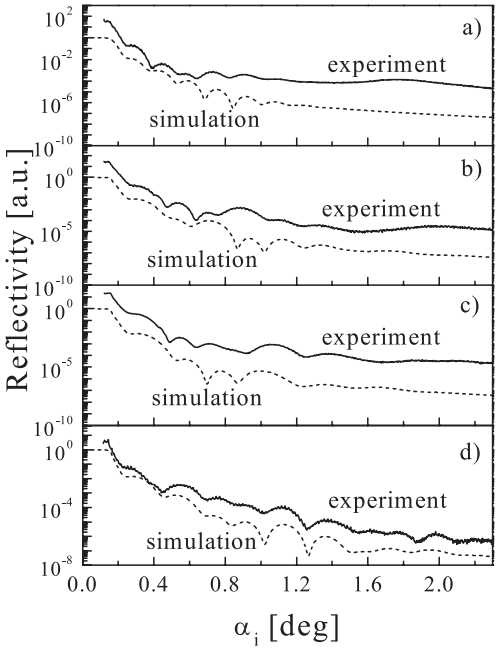

Fig. 3. X-ray reflectivity measurements for three heterostructures together with the SRO "thin" film: a) refers to the SRO film while b), c) and d) refer to the 11/5/11, 9/9/9 and 7/13/7 heterostructures respectively. Theoretical curves are also shown by dashed lines.

of Figure 1. It can be noticed that the overall resistance behaviour is comparable with that of single crystal samples (300 $\mu\Omega$ cm at 300 K [25,26]) and the fingerprint of a magnetic transition can be clearly noticed at about 140 K (160 K for single crystal samples [25,26]).

Once we checked the strict correspondence between RHEED oscillations and the growth of a single unit cell of SRO, we started to engineer various SRO/STO heterostructures consisting of ultrathin blocks, a few unit cells thick, using the *in situ* RHEED diagnostic. We grew three different $(SRO)_M/(STO)_N/(SRO)_M$ heteroepitaxial structures ($M/N/M$ structures), consisting of N unit cells of STO sandwiched between M unit cells of SRO: namely 11/5/11, 9/9/9 and 7/13/7 heterostructures. The total thickness was maintained constant ($N + 2M = 27$ for all heterostructures). A SRO thin film, having approximately the same overall thickness, was grown for the purpose of comparison. In Figure 3 specular X-ray reflectivity measurements are shown for all three heterostructures together with the SRO thin film: a) refers to the SRO film while b), c) and d) refer to the 11/5/11, 9/9/9 and 7/13/7 heterostructures respectively. Theoretical curves were obtained using the simulation program described in references [18,19]. Input parameters of this program are the same as before with the exception of the thickness of each constituent block and the roughness of each interface. From Figure 3, it can be seen that, even thought the overall thickness for all samples are nearly the same, the specific features of the experimental reflectivity spectrum vary from sample to sample. Such an effect must be ascribed to the differences in the individual layer

Table 1. Individual layers thickness, surface and interface roughness deduced by X-ray reflectivity measurements.

Sample SRO/STO/SRO nominal u.c.	Thickness SRO/STO/SRO (Å) ±2 Å	RMS surface roughness (Å)±1 Å	RMS interface roughness (Å) ±1 Å
156/-/-	618/-/-	9	-
-	134/-/-	9	-
11/5/11	45/18/45	7	5
9/9/9	33/32/33	9	5
7/13/7	28/51/28	6	4

thickness and interface roughness of the various samples. Theoretical simulation curves agree quite well with the experimental data. Using the theoretical curves shown in Figure 3 we deduced, for all the samples, the overall thickness, the surface roughness, the thickness of each block and the roughness of the interfaces. All values are reported in Table 1. From the table it can be noticed that the surface roughness of the thin SRO films and the SRO/STO heterostructures is the same, within the experimental error, as the roughness of the SRO film 620 Å thick, namely about 2 unit cells. This result suggests that such roughness may be an intrinsic property of the surface (perhaps caused by the exposure of surface to air) rather than being a cumulative effect of the growth process. Thickness of the individual blocks, as deduced from the theoretical simulation, is in good agreement with the thickness expected on the basis of the RHEED oscillations. The interface roughness is, for all samples, of the order of a single unit cell. This finding indicates that ultrathin blocks, a few unit cell thick, can be engineered with the precision of a single unit cell. The above results are confirmed by the diffraction measurements in specular configuration reported in Figure 4. Diffraction spectra were recorded in a narrow angular range around the (002) peak of the substrate (the intense peak indicated by an asterisk in the figure). As for Figure 3, a) refers to the SRO film while b), c) and d) refer to the 11/5/11, 9/9/9 and 7/13/7 heterostructures, respectively. Experimental data reported in Figure 4 were simulated using a program based on the Takagi-Taupin equation of dynamical theory [20,21]. In the case of the SRO film the faint intensity oscillations seen in the experimental spectrum (Fig. 4a) originate from finite size effects and allow the estimation of the overall film thickness. In the case of the $M/N/M$ heterostructures the intensity modulation is much more evident and is caused by interference effects between the different heteroepitaxial blocks. Such diffraction patterns are very sensitive to small variations in the thickness of each individual block. Indeed, the $SrRuO_3$ layers splits the diffraction pattern into two peaks (Fig. 4b) because of interference effects typical of sandwiched structures [27–29]. Modulation becomes more pronounced for thicker STO layers, as shown in Figures 4c and d. The angular position of the interference fringes depends on the SRO lattice constant as well as on the thickness of the STO barrier. Therefore, not only the thickness of the barrier layer, but also the c-axis parameter of SRO, can be obtained fitting the full diffraction curve. Theoretical simulation spectra shown in Figure 4 fit

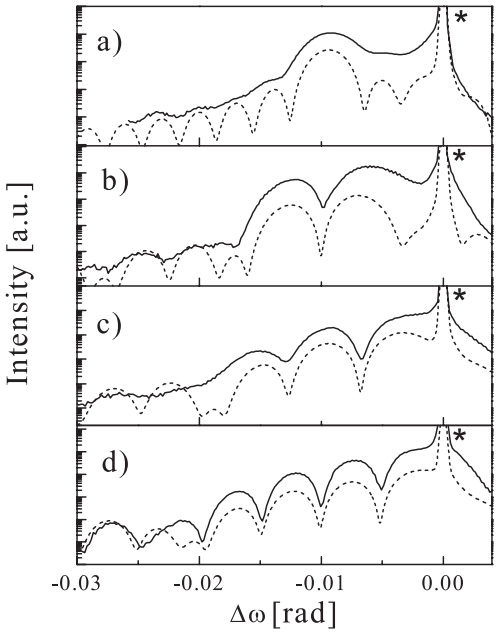

Fig. 4. Diffraction spectra in a narrow angular range around the (002) peak of the STO substrate (indicated by an asterisk): a) refers to the SRO "thin" film while b), c) and d) refer to the 11/5/11, 9/9/9 and 7/13/7 heterostructures, respectively. On the x-axis, the relative angular distance respect to the peak of the STO substrate is reported. Theoretical curves, indicated by dashed lines, are obtained assuming the individual layer thickness deduced from RHEED measurements.

the experimental data very well. They were obtained using the thickness values expected on the basis of RHEED oscillations, namely: b) 11/5/11, c) 9/9/9 and d) 7/13/7. The c-axis lattice parameters of the SRO blocks, utilized to simulate the theoretical curves shown in Figure 4, are reported in Figure 5a. Reciprocal space maps, recorded with a point detector under grazing incidence diffraction geometry (angle of incidence 0.1°), were used to measure the in-plane axis parameters (reported in Fig. 5b). These measurements were performed around the (022) and (202) reciprocal lattice points of the substrate and the film to determine separately both the a and b lattice parameters reported in Figure 5b. The straight full line in Figure 5b indicates the lattice parameter of the STO substrate. From Figure 5 it can be noticed that all heterostructures show an orthorhombic distortion which decreases with the increasing of the thickness of the STO layer. Values of the

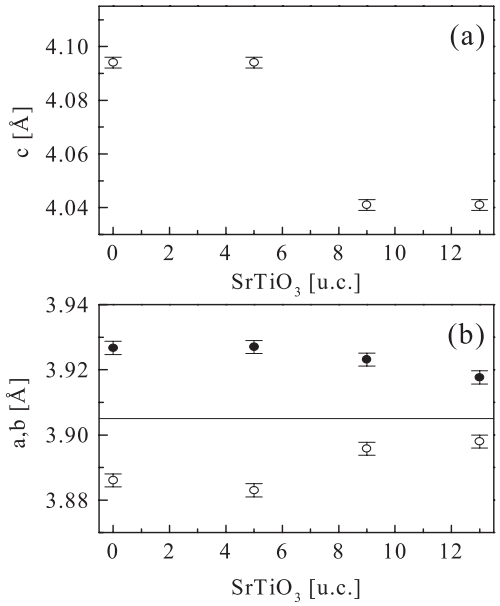

Fig. 5. (a) *c*-axis lattice parameters of the SRO blocks, deduced from the diffraction measurements shown in Figure 4. (b) In-plane lattice parameters for the "thin" film and the different heterostructures deduced from reciprocal space maps. The straight line indicates the lattice parameter of the STO substrate. On the x axis the thickness of the STO barrier is reported in number of unit cells (u.c.).

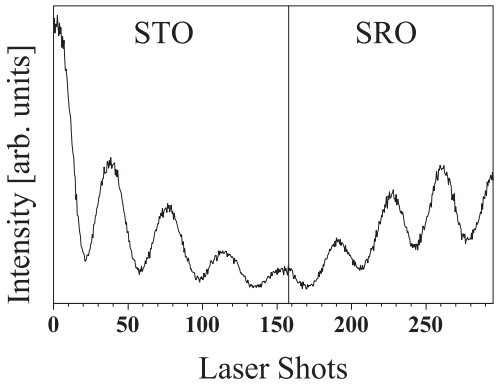

Fig. 6. RHEED oscillations during a single deposition cycle of a 4×4 superlattice.

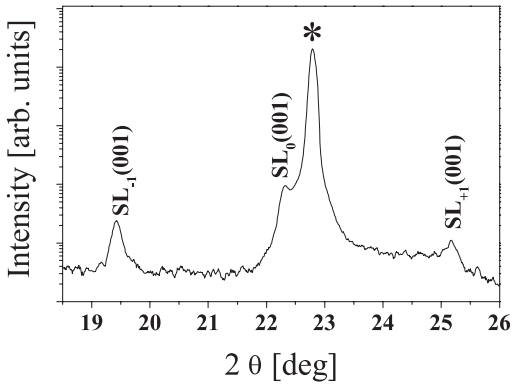

Fig. 7. Diffraction spectrum of the same 4×4 superlattice shown in Figure 6 in the proximity of the (002) diffraction peak of the STO substrate (indicated by an asterisk).

c lattice parameter for SRO thin films are larger than that found in the case of the 600 Å thick film. This finding can be, at least partially, explained by an in-plane compressive epitaxial strain. Further details on the structure of these ultrathin heterostructures and on their epitaxial relationship with the STO substrate will be given elsewhere [30].

Finally, we grew by laser MBE various superlattices consisting of M layers of SRO and N layers of STO alternately stacked in sequence $([(\mathrm{SRO})_M/(\mathrm{STO})_N]_{15}$ superlattices where the deposition cycle is repeated 15 times). In Figure 6, RHEED oscillations are shown for a 4×4 superlattice during an individual cycle of the superlattice deposition. The change of the average intensity of the specular spot can be possibly ascribed to the different electron scattering factors of atoms in the two compounds and to the phase shift caused by the slightly different step heights between SRO and STO. No sizeable decay of the oscillation amplitude is observed during the growth of successive bilayers. $\theta - 2\theta$ X-ray diffraction measurements of the superlattices were carried out with a standard Bragg-Brentano diffractometer using Cu-K_α radiation ($\lambda = 1.5405$ Å). In Figure 7 the diffraction spectrum of a 4×4 superlattice is shown in the proximity of the (002) diffraction peak of the STO substrate (indicated by an asterisk in the figure). The angular distance between the SL_{-1} and SL_{+1} satellite peaks allows the deduction of the modulation length Λ of the superlattice using the formula $\Lambda = \lambda/(\sin\theta_{+1} - \sin\theta_{-1})$, where $\theta_{\pm 1}$ represent the angular positions of the first order satellite peaks. Using the above formula a Λ value of 31.35 Å was estimated. Such a value can be compared with the estimate of 31.8 Å obtained by the formula $\Lambda = Mc_1 + Nc_2$, where c_1 and c_2 represent the lattice parameters of the two constituent blocks (assumed to be 4.0 Å and 3.9 Å, for SRO and STO respectively). This result shows, once more, the very good reliability of the RHEED technique for the *in situ* diagnostic of the growth of heterostructures and superlattices based on perovskite oxides.

4 Conclusions

It is experimentally difficult to establish the true nature of transport across a junction. For tunneling current to dominate the junction conduction, a very thin barrier is mandatory. Typically, a true quantum mechanical tunnel becomes observable only for a barrier thickness no larger than 20 Å which corresponds to approximately five perovskite unit cells. Tunneling decreases exponentially with the barrier thickness. In practice, because of the interface roughness, thicker barriers, usually in the range $30 - 50$ Å are used to prevent shorts between the magnetic electrodes. It is clear that an important goal in this field would be to engineer true tunnel junctions based on perovskite heterostructures where the thickness and the

interface roughness of the barrier are controlled at the level of a single unit cell. Pulsed laser deposition with *in situ* RHEED technique seems to offer such a possibility. Namely, we have shown that high quality heterostructures and superlattices based on SRO and STO individual blocks can be grown in a purely 2D, layer by layer mode using laser MBE. A detailed investigation carried out at the ESRF synchrotron facility by various X-ray diffraction techniques has demonstrated that the intensity oscillations of the RHEED spots correspond strictly to the growth of a single perovskite unit cell, either SRO or STO. Using the RHEED technique ultrathin STO barriers (down to five unit cells) were engineered with a control of the thickness of each layer at the level of a single unit cell. In these structures the interfaces between the different constituent blocks result to be very sharp with a roughness of about one unit cell.

We would like to thank the staff of the ID32 beamline at ESRF and in particular J. Zegenhagen and T.L. Lee for their suggestions during the measurements.

References

1. A. Gupta, J.Z. Sun, J. Mag. Mag. Mater. **200**, 24 (1999)
2. J.Z. Sun, W.J. Gallagher, P.R. Ducombe, L. Krusin-Elbaum, R.A. Altman, A. Gupta, Y. Lu, G.Q. Gong, G. Xiao, Appl. Phys. Lett. **69**, 3266 (1996)
3. Y. Lu, X.W. Li, G.Q. Gong, G. Xiao, A. Gupta, P. Lecoeur, J.Z. Sun, Y.Y. Wang, V.P. Dravid, Phys. Rev. B **54**, R8357 (1996)
4. J.H. Park, E. Vescovo, H.J. Kim, C. Kwon, R. Ramesh, T. Venkatesan, Nature **392**, 794 (1998)
5. J. O'Donnel, A.E. Andrus, S. Oh, E.V. Colla, J.N. Eckstein, Appl. Phys. Lett. **76**, 1914 (2000)
6. J.H. Guus, M. Rijnders, G. Koster, D.H.A. Blank, H. Rogalla, Appl. Phys. Lett. **70**, 1888 (1997)
7. P.A. Salvador, A.M. Haghiri-Gosnet, B. Mercey, M. Hervieu, B. Raveau, Appl. Phys. Lett. **75**, 2638 (1999)
8. G. Balestrino, S. Lavanga, P.G. Medaglia, P. Orgiani, A. Tebano, Phys. Rev. B **64**, 20506 (2001)
9. T. Terashima *et al.*, Phys. Rev. Lett. **65**, 2684 (1990)
10. M. Varela *et al.*, Phys. Rev. Lett. **86**, 5156 (2001)
11. T. Haage, J. Zegenhagen, H.-U. Habermeier, M. Cardona, Phys. Rev. Lett. **80**, 4225 (1998)
12. V.S. Achutharaman, N. Chandrasekhar, O.T. Valls, A.M. Goldman, Phys. Rev. B **50**, 8122 (1994)
13. G.S. Gausepohl, M. Lee, K. Char, R.A. Rao, C.B. Eom, Phys. Rev. B **52**, 3459 (1995)
14. P.B. Allen *et al.*, Phys. Rev. B **53**, 4393 (1996)
15. X.D. Wu, S.R. Foltyn, R.C. Dye, Y. Coulter, R.E. Muenchausen, Appl. Phys. Lett. **62**, 2434 (1993)
16. J. Lin *et al.*, Appl. Phys. Lett. **76**, 2430 (2000)
17. H. Kawasaki *et al.*, Science **266**, 1540 (1994)
18. D.L. Windt, Comput. Phys. **12**, 360 (1998)
19. M. Sànchez del Rìo, R.J. Dejus, SPIE Proc. **3448**, 340 (1998)
20. S. Takagi, J. Phys. Soc. Jpn **26**, 1239 (1969)
21. D. Taupin, Bull. Franc. Minér. Crist. **87**, 469 (1964)
22. J. Choi, C.B. Eom, G. Rijnders, H. Rogalla, D.H.A. Blank, Appl. Phys. Lett. **79**, 1447 (2001)
23. J.P. Maria, S. Trolier-McKinstry, D.G. Schlom, M.E. Hawley, G.W. Brown, J. Appl. Phys. **83**, 4373 (1998)
24. P. Orgiani, C. Aruta, G. Balestrino, S. Lavanga, P.G. Medaglia, A. Tebano, Eur. Phys. J. B **26**, 25 (2002)
25. A. Callaghan, C.W. Moeller, R. Ward, Inorg. Chem. **5**, 1572 (1966)
26. J.M. Longo, P.M. Raccah, J.B. Goodenough, J. Appl. Phys. **39**, 1327 (1968)
27. G.T. Baumbach, H. Rhan, U. Pietch, Phys. Stat. Sol (a) **109**, K7 (1988)
28. L. Tapfer, K. Ploog, Phys. Rev. B **40**, 9802 (1989)
29. X. Chu, B. Tanner, Appl. Phys. Lett. **49**, 1773 (1986)
30. C. Aruta *et al.*, to be published